HHS Public Access

Author manuscript

Nat Methods. Author manuscript; available in PMC 2013 November 01.

Published in final edited form as:

Nat Methods. 2013 May ; 10(5): 421–426. doi:10.1038/nmeth.2411.

Single Molecule Imaging of Transcription Factor Binding to DNA in Live Mammalian Cells

J Christof M Gebhardt[1,6], **David M Suter**[1,6], **Rahul Roy**[1,4], **Ziqing W Zhao**[1,2], **Alec R Chapman**[1,2], **Srinjan Basu**[1,3,5], **Tom Maniatis**[3], and **X Sunney Xie**[1]

[1]Department of Chemistry and Chemical Biology, Harvard University, Cambridge, Massachusetts, USA

[2]Graduate Program in Biophysics, Harvard University, Cambridge, Massachusetts, USA

[3]Department of Biochemistry and Molecular Biophysics, Columbia University Medical Center, New York, New York, USA

Abstract

Imaging single fluorescent proteins in living mammalian cells is challenging due to out-of-focus fluorescence excitation by common microscopy schemes. We report the development of a novel fluorescence microscopy method, reflected light sheet microscopy (RLSM), which allows selective plane illumination throughout the nucleus of living mammalian cells, for reducing out-of-focus fluorescence signal. Generation of a thin light sheet parallel to the imaging plane and close to the sample surface is achieved by reflecting an elliptical laser beam incident from the top by 45° with a small mirror. The thin light sheet allows for an increased signal-to-background ratio superior to previous illumination schemes and enables imaging of single fluorescent proteins with up to 100 Hz time resolution. We demonstrate the sensitivity of RLSM by measuring the DNA-bound fraction of glucocorticoid receptor (GR) and determine the residence times on DNA of various oligomerization states and mutants of GR and estrogen receptor (ER), enabling us to resolve different modes of DNA binding of GR. Finally, we demonstrate two-color single molecule imaging by observing the spatio-temporal co-localization of two different protein pairs. The combination of our single molecule measurements and statistical analysis reveals dynamic properties of transcription factors in live mammalian cells.

Correspondence should be addressed to X.S.X, xie@chemistry.harvard.edu.

[4]Current address: Department of Chemical Engineering, Indian Institute of Science, Bangalore, India

[5]Current address: Department of Biochemistry, University of Cambridge, Cambridge, United Kingdom

[6]These authors contributed equally to this work

Author contributions

J.C.M.G. conceived and set up the RLS microscope. J.C.M.G. and D.M.S. designed experiments and data analysis. D.M.S. cloned fusion proteins, established cell lines and contributed to measurements. J.C.M.G. and R.R. cloned mEos2-GR and mEos2-H4, J.C.M.G. performed measurements and analyzed data. R.R., Z.W.Z. and A.C. contributed to system setup. R.R. and Z.W.Z. contributed to light sheet characterization. R.R. and A.C. contributed analysis code. S.B. contributed to cloning. R.R., Z.W.Z. and S.B. contributed cells for initial performance tests. X.S.X. initiated the project. X.S.X. and T.M. supervised the project. J.C.M.G., D.M.S. and X.S.X. wrote the manuscript with contributions from all authors.

Introduction

Tracking single molecules in living cells provides a direct way to probe the kinetics of their interactions with other cellular components and is particularly useful to characterize unsynchronized dynamic events[1]. This applies well to the study of mammalian transcription factors, which have recently been shown to interact with DNA in a very dynamic manner[2] and thus ask for new models of transcription initiation[3]. Imaging single fluorescent fusion proteins has provided valuable insight into the dynamic properties of transcription and translation in living bacterial cells[4, 5]. However, it remains challenging to observe biomolecules at the single molecule level in the nuclei of living mammalian cells.

While low concentrations of single intracellular fluorescent molecules can be visualized using wide-field illumination[6, 7], distinguishing higher concentrations of single molecules requires a reduction of the excitation volume. Total internal reflection fluorescence (TIRF) microscopy illuminates a thin section close to the sample surface, and enables visualization of single fluorescent molecules in the cell membrane[8]. However, selective excitation in the cell nucleus cannot be achieved with TIRF. An increase in signal-to-background ratio (SBR) has been achieved with highly inclined and laminated optical sheet (HILO) microscopy[9]. Unfortunately, reduction of the light sheet thickness in HILO is proportional to a decrease of the illuminated area in the focal plane. Moreover, the inclined nature of the illuminating laser beam still leads to out-of-focus fluorescence excitation.

The recently developed selective plane illumination scheme allows for further reduction of the illuminated volume and restricts sample excitation to the focal plane[10]. This principle has been used to image living embryos with minimal photodamage by illuminating the sample from the side with an objective placed orthogonal to the detection objective[10]. Subsequently, diffusion of single quantum dots was imaged in developing zebrafish[11], diffusion of dye-labeled single molecules was observed in real time in large salivary gland nuclei[12] and super-resolution microscopy was performed with photoactivatable fluorescent proteins in cellular spheroids[13]. In order to image small mammalian cells with selective plane illumination, two objectives with low numerical aperture were used to section the cell at 45° with respect to the sample surface[14, 15]. Using a similar arrangement of objectives, the light sheet was recently replaced by an illumination scheme based on Bessel beams[16]. However, single molecule detection has not yet been reported with this configuration of objectives, probably because only objectives with low numerical aperture of < 0.8 that are not optimal for single molecule imaging can be used.

Here we report a novel illumination scheme that combines selective plane illumination with a vertical arrangement of illumination and detection objectives. In this new geometry, a disposable mirror reflects the light sheet into a horizontal plane close to the sample surface, thus allowing horizontal sectioning of the cells and the use of a high numerical aperture objective for fluorescence detection. With our setup we achieve single fluorescent protein imaging in live mammalian cells with high SBR and millisecond time resolution.

We demonstrate the potential of our new microscopy method, reflected light sheet microscopy (RLSM), by directly monitoring the binding properties of fluorescently labeled

glucocorticoid receptors (GR) and estrogen receptors (ER) to DNA. GR is a transcription factor that localizes mostly to the cytoplasm in the absence of hormone but forms homodimers and translocates into the nucleus upon binding to glucocorticoids[17]. Previous studies have shown that dimeric GR binds directly to DNA at regulatory sequences, while the monomer can be indirectly recruited to DNA by other DNA-bound protein complexes[18]. The mode of DNA interaction defines whether the target gene is activated or repressed. We find a 10-fold decrease in residence time for monomeric GR compared to the dimeric transcription factor, and a two-fold shorter residence time for indirectly bound GR. A similar result is obtained for ER. Finally, we demonstrate the capability of RLSM for two-color single molecule imaging. This allows us to directly observe spatio-temporal co-localization of GR and its coactivator GRIP1 and of the heterodimeric transcription factor pair BMAL1 and CLOCK. The imaging technique described here will be generally applicable to single molecule studies in living mammalian cells.

Results

Setup of the reflected light sheet microscope

In selective plane illumination microscopes, two orthogonal objectives are used[19]. Due to spatial constraints imposed by the objectives, the light sheet can only be positioned at distances > 10 μm above the sample surface, and the full width at half maximum (FWHM) of the light sheet is > 2 μm[12]. Selective illumination of typical mammalian cell nuclei is not possible with this geometry. We overcame this problem by replacing the condenser of an inverted microscope with a vertically mounted high numerical aperture (NA) water immersion objective (Fig. 1a, see online methods, Supplementary Fig. 1 and Supplementary Video 1). This objective focuses an elliptical laser beam incident from the top to form a diffraction-limited sheet of light with a FWHM of > 0.5 μm (Fig. 1b). A small mirror reflects the light sheet by 90° and projects it horizontally into the nucleus of the cell, thus allowing sub-micrometer optical sectioning. Vertical scanning is achieved by mounting the sample on a xyz piezo stage. Wide-field imaging of fluorescent light by a second high NA objective enables high sensitivity and temporal resolution. Due to the upright geometry of illumination and detection objectives, standard glass bottom dishes can be used to both grow and image mammalian cells, thereby simplifying experimental procedures.

We used a disposable tipless atomic force microscopy (AFM) cantilever coated with an aluminum layer to reflect the laser beam (see online methods). We used the signal from small fluorescent beads to compare the dimensions of the laser beam in the vicinity of the focus before and after reflection (Fig. 1b, see online methods and Supplementary Fig. 2). As expected, the reflection does not alter the shape of the laser beam. Different AFM cantilevers showed a similar performance (data not shown). By changing the dimensions of the incident beam with a spherical aperture in front of the focusing objective, the Rayleigh length over which the light sheet maintains a relatively constant thickness can be controlled (Fig.1b). Due to the shape of the light sheet, a small gap between surface and light sheet cannot be illuminated (Fig. 1b). Measurements were performed at an aperture size of 4 mm, corresponding to a FWHM of the light sheet of ~ 1 μm and a Rayleigh length of ~ 11 μm.

We compared the single molecule detection capability of our new microscopy method, RLSM, with HILO illumination. For the HILO measurements, we chose a small illumination area of ~ 10 μm to keep the light sheet thickness small (~ 5 μm)[9]. We expressed histone H4 fused to the photoactivatable fluorescent protein mEos2 in MCF-7 cells (see online methods). We activated a subset of mEos2 molecules with a 405 nm laser in HILO illumination mode, and subsequently imaged the fluorescence excited with a 560 nm laser by alternating every 50 ms between RLSM and HILO modes. At low mEos2 activation and close to the coverslip, RLSM increased the SBR by 1.5±0.1 fold (±s.e.m., n = 3504 molecules, 8 cells) compared to HILO (Fig 1c and online methods). At high activation densities, the SBR ratio between RLSM and HILO increased to 5.3 ±0.4 (±s.e.m., n = 267 molecules, 3 cells, Supplementary Fig. 3). Moreover, RLSM allows detection of single molecules throughout the cross-section of the nucleus, while the illuminated area is restricted to a central part of the cross-section for HILO (Fig. 1c). We confirmed the superior SBR and field of view of RLSM throughout the nucleus in different z-sections (Supplementary Fig. 4).

DNA-bound fractions of transcription factors

We tested different fluorescent fusion partners for single molecule observations in living cells. In principle, the protein fusion tags SNAP and Halo, which can be covalently labeled with organic dyes, are a very attractive labeling strategy because of the brightness and photostability of organic dyes[20–22]. Unfortunately, we found that both SNAP and Halo proteins exhibit stable binding events in the nucleus (Supplementary Videos 2 and 3). This intrinsic binding will bias the kinetic analysis of DNA interactions of protein fusion partners. We therefore chose the bright fluorescent proteins mEos2 and YPet as labels for transcription factors, as neither of them showed nuclear binding (Supplementary Videos 4 and 5). In addition, we used the fluorescent proteins eGFP and TagRFP-T as candidates for two-color applications due to their spectral separation.

To study the diffusion of glucocorticoid receptor (GR) in the nucleus, we expressed a mEos2-GR fusion protein in MCF-7 cells with and without treatment with 100 nM of the hormone analog dexamethasone. We photoactivated only a small subset of mEos2 molecules in the focal plane to limit the number of simultaneously observable molecules and thereby avoid overlap of their trajectories[23], and imaged single fluorescent proteins with 10 ms time resolution (Supplementary Video 6).

We analyzed the diffusion trajectories of nuclear GR (Fig. 2a). Each time a molecule was photoactivated in the field of view, we determined the cumulative distribution function of its squared displacement during a fixed time interval of 10 ms (see online methods)[24]. We observe a higher fraction of small displacements for induced GR in the presence of 100 nM dexamethasone compared to uninduced GR (Fig. 2b). The cumulative distribution functions deviate from an exponential form expected for Brownian motion (Equation (1) in online methods). This suggests that a GR molecule undergoes transitions between different states (unbound and bound to DNA) with different diffusion constants. Both distributions can be well fit with three exponential components, corresponding to three effective diffusion constants $D_{1\text{-}3}$ (Equation (2) in online methods). We measured D_1 = (0.13± 0.03) μm^2 s^-

((12± 2)%), D_2 = (1.6± 0.3) μm^2 s$^-$ ((52±5)%) and D_3 = (8.9±3.0) μm^2 s$^-$ ((36±6)%) for uninduced GR and similar values of D_1 = (0.13 ± 0.01) μm^2 s$^-$ ((37±2)%), D_2 = (1.4±0.2) μm^2 s$^-$ ((37±3)%) and D_3 = (9.2±2.3) μm^2 s$^-$ ((26±4)%) for induced GR. A recent study on dye-labeled STAT1 observed effective diffusion constants in the nucleus that are very similar to those reported here[25].

To assign the slow component, we repeated the measurement for a fusion protein of mEos2 to histone H4, which is stably incorporated into chromatin (Fig. 2b). We again found three diffusion components, with the slowest component D_1 = (0.13±0.01) μm^2 s$^-$ having the highest weight of (71±4)%. The movement of chromatin in mammalian cells has been observed, with diffusion constants ranging from 10^{-4} to 10^{-3} μm^2 s$^-$ [26], slower than D_1. We calculated a localization error of Δx= 49 nm at the photon count of 27.5 within 10 ms for H4[27]. Such average displacement corresponds to an apparent diffusion constant of 0.06 μm^2 s$^-$ close to D_1. Thus we conclude that the apparent slow component arises from the localization uncertainty of DNA-bound fluorescent molecules at low signal levels. The larger effective diffusion constants presumably arise from transient non-specific interactions with DNA and spatially restricted diffusion in the nucleus[28].

We used the weight of the slowest diffusion component as an estimate for the DNA-bound fraction of the transcription factor. Accordingly, 12% of residual nuclear GR is bound to chromatin in the absence of hormone treatment, compared to 37% after dexamethasone induction. These values are similar to previous estimates for the DNA bound fraction of nuclear STAT1 and p53[22, 25]. On a single molecule basis, these percentages correspond to the fractions of time a GR is bound to DNA.

DNA residence times of transcription factors

Next we measured the *in vivo* residence time of individual GR dimer molecules bound to DNA in the presence of 100 nM dexamethasone, using the principle of detection by localization[29]. Since mEos2 exhibits prolonged fluorescent dark states that might interfere with residence time measurements, we here used the bright yellow fluorescent protein YPet as a tag for GR, in a plasmid allowing low expression levels in MCF-7 cells (see online methods). We considered a molecule to be bound to DNA only if it stayed immobile for at least two consecutive frames (Supplementary Video 7 and online methods)[29].

Due to the fast photobleaching of fluorescent proteins, it is not possible to determine the residence time based on continuous single molecule tracking, since both photobleaching and dissociation contribute to the loss of the fluorescent signal. Instead, we performed time-lapse illumination with a fixed camera integration time τ_{int} of 50 ms interspersed with dark periods of varying duration τ_d (Fig. 3a). This enabled us to extract the dissociation rate constant k_{off} and photobleaching rate constant k_b from the effective off-rate constant k_{eff} obtained from distributions of the measured fluorescent ‘on’ times of bound YPet-GR (see online methods). We obtained k_{off} = (0.69 ± 0.11) s$^-$ and k_b = (26.8 ± 0.5) s$^-$ for dimeric GR. The GR residence time of 1.45 s (calculated as k_{off}^-, see Supplementary Table 1) falls in the same range as the fluorescence recovery time of 5 s initially measured in fluorescence recovery after photobleaching (FRAP) experiments[2, 30] and is similar to the residence times of dye-labeled STAT1 and p53 recently obtained in single molecule experiments[22, 25]. The

k_b of YPet is consistent with the value we found in a control experiment performed *in vitro* under comparable illumination conditions (Supplementary Fig. 5).

We then probed DNA binding of the monomeric GR by using a point mutant capable of nuclear import upon induction but incapable of dimerization (GR A458T)[31]. Interestingly, a simple model with one dissociation rate constant was not sufficient to fit the fluorescent 'on' time distributions of GR A458T (Supplementary Fig. 6). We therefore used a model describing a transcription factor that has two populations with different dissociation rate constants $k_{off,1}$ and $k_{off,2}$ and amplitudes A_1 and A_2 (Equation (4) in online). We found that (97±2)% of GR A458T has a residence time of (0.15 ±0.02) s, 10-fold faster than dimeric GR, and a second fraction of (3±2)% with a residence time of (0.76 ± 0.12) s (Fig. 3c and Supplementary Fig. 7). To assign these components, we imaged a GR mutant lacking the DNA binding domain (GR ΔDBD), which exhibited a single residence time of (0.76 ± 0.35) s, comparable to the slow fraction of GR A458T (Supplementary Fig. 7 and 8). We therefore conclude that the 3% component of monomeric GR A458T molecules represents protein-protein interactions, not direct binding to DNA.

Next, we measured the residence time of the closely related estrogen receptor-α (ER) fused to YPet. Similar to GR, ER can be induced by hormone treatment to dimerize and bind to cognate DNA sequences. In contrast to GR, ER is constitutively localized to the nucleus in MCF-7 cells[32]. Similar to GR, we resolved a large fraction ((87 ± 5)%) of uninduced ER dissociating at a rate constant six-fold faster than the dimeric ER (Fig. 3 and Supplementary Fig. 9). Taken together, these results suggest that our method allows us to discriminate between three different modes of DNA binding, i.e., dimeric, monomeric, and indirect DNA binding through association with other transcription factors.

Spatio-temporal co-localization of two molecular species

We next demonstrated spatio-temporal co-localization of GR and GRIP1 on DNA. GRIP1 is a co-activator for GR and other steroid receptors[33]. We performed the experiments in U2-OS cells that are commonly used for GR and GRIP1 studies since they do not express these factors endogenously[34]. This allows the exclusive expression of fluorescently labeled GR and GRIP1. YPet fusions of both proteins showed residence times comparable to GR measured in MCF-7 cells (Supplementary Table 1 and Supplementary Fig. 9). For simultaneous observation of GR and GRIP1, we performed two-color single molecule imaging by labeling GRIP1 with eGFP and GR with TagRFP-T. We alternated 488 nm and 560 nm laser excitation with 50 ms integration time in the same light sheet illumination plane (Supplementary Video 8). Figure 4a shows an example of spatio-temporal co-localization of GR and GRIP1 on DNA. By comparing the numbers of localizations per pixel and second of GR and GRIP1 without visible partner with the number of detected co-localization events we estimate that co-localization was ~ 80 times more likely then expected by chance.

Next, we used the same fluorescent proteins to label BMAL1 and CLOCK, a transcription factor pair known to bind DNA as a heterodimer[35]. Both proteins show co-localization events, consistent with the formation of a complex composed of BMAL1, CLOCK and largely stationary DNA (Fig. 4b and Supplementary Video 9). As for GR and GRIP1, co-

localization events were two orders of magnitude more likely then expected by chance. Thus, RLSM can be used to probe the spatio-temporal co-localization of two different molecular species labeled with a fluorescent protein at the single molecule level.

Discussion

We report a novel microscopy scheme based on selective plane illumination, capable of resolving individual fluorescent proteins in the nucleus of living mammalian cells. The vertical orientation of the illumination and detection objectives in our microscope introduces several advantages compared to the orthogonal geometry of objectives normally employed in selective plane illumination instruments[19]. First, any commercial inverted microscope may be switched to a light sheet illumination setup by adjusting the laser illumination beam path, replacing the condenser with a water dipping objective and connected mirror and exchanging the sample stage with a piezo stage. Second, both objectives can be chosen with high numerical aperture. This allows for a very thin excitation light sheet (> 0.5 μm) as well as a high efficiency of fluorescent light collection with the detection objective. Third, the reflecting mirror allows positioning of the horizontal light sheet close to the cover glass surface, leaving only a small gap of ~ 2 μm which cannot be illuminated. This gap is small enough to enable sectioning of most of the nucleus of mammalian cells, resulting in a high SBR of fluorescence imaging superior to wide field and HILO illumination. Finally, there is no need for special observation chambers, as commercially available glass bottom culture dishes can be used for both cell culture and imaging, further simplifying experimental procedures[14, 15].

RLSM allowed to directly observe the DNA binding of GR and ER labeled with a fluorescent protein at the single molecule level. The residence times we obtained by this method are comparable to values recently found for single dye-labeled STAT1 and p53 that could be continuously observed due to the superior photostability of organic dyes[22, 25]. The time-lapse approach we used allows reliable measurements of residence times ranging from 50 ms (as given by the integration time) and several seconds. For longer time scales, this approach is limited, since cellular movements prevent the reliable assignement of a continuously binding molecule.

The increase in residence time of dimeric GR and ER compared to the monomeric transcription factor probably reflects stabilization of DNA binding by an associated partner. However, our observations are also compatible with a proportion of molecules remaining in the monomeric form, since the dynamics of a fast dissociating fraction of molecules cannot be resolved if the majority of molecules dissociates slowly (Supplementary Fig. 6). In contrast, a small fraction of longer bound molecules was resolved for monomeric GR and ER, which we could assign to an indirect binding mode to other protein factors for GR.

A common technique to study transcription factor dynamics is FRAP, which monitors the recovery of fluorescence in a bleached area. This area is replenished through diffusion and rebinding of unbleached fluorescent fusion proteins, which replace dissociated bleached molecules. Using FRAP, an upper bound for the residence time of GR of 170 ms has been reported[36], nine-fold faster than we measured for dimeric GR. However, the indirect

assessment of residence times via reaction-diffusion models is error-prone, as experimental conditions including the geometry of the bleached volume, the fraction of free diffusing molecules and photophysical properties of the fluorophore must be accurately determined[22, 36–40]. The direct determination of transcription factor residence times by single molecule approaches is not subject to these limitations. In addition, the single molecule trajectories accessible with our method allow nanometer spatial and millisecond temporal accuracy of a molecular species.

With the novel technique described here we were able to quantitatively measure binding fractions and residence times, and distinguish different modes of transcription factor binding to DNA. Furthermore, we demonstrated the potential of RLSM to perform simultaneous imaging of two different molecular species at the single molecule level. These types of real-time single molecule experiments will allow detailed mechanistic studies of transcription initiation, and provide the opportunity to probe the dynamical properties of molecular interactions *in vivo*.

Online Methods

Optical setup of RLSM

The reflected light sheet microscope is integrated into an inverted microscope (IX71, Olympus)(Supplementary Fig. 1a). Illumination lasers (405 nm, 50 mW, Electra-40, Laserglow; 488/514 nm, 1000 mW, Innova300, Coherent; 560 nm, 1000 mW, VFL-P-1000-560, MPB communications; actual intensity was set to 3 mW in the sample plane) are collimated and co-linearly combined via dichroic beamsplitters. Shutters (LS3M2, Uniblitz) are used to control the active laser times. A telescope of two cylindrical lenses (f = 40 mm, LJ1402L1-A and f = 400 mm, LJ1363L1-A, both Thorlabs) creates an expanded and collimated line that overfills the back aperture of the vertical illumination objective (LUMPLFLN 40x W, NA 0.8, Olympus) and is focused to a diffraction limited light sheet. A third cylindrical lens (f = 150 mm, LJ1629L1-A, Thorlabs) is used to control the lateral extension of the light sheet. A spherical iris in front of the illumination objective allows reduction of the illumination line dimensions and thus the FWHM of the light sheet. A tipless AFM cantilever (HYDRA2R-100N-TL-10, Nanoscience) is mounted to the illumination objective via a custom designed holder (Supplementary Fig. 1b and 1c). The disposable AFM cantilever is custom-coated with a 1 nm Ti layer followed by 40 nm Al layer by thermal evaporation. A manual xy-stage (ST1XY-S, Thorlabs) and a z-stage (423, Newport) allow simultaneous positioning of illumination objective and cantilever holder with respect to the detection objective (UPlanApo 100x 1.35 Oil or UPlanSApo 100x 1.4 Oil, both Olympus). Fluorescent light (filters sets for mEos2: dichroic Di01-R561, filters Brightline 617/73 and Edgebasic long wave pass 561, Semrock; YPet: dichroic FF495-Di03, Semrock and filter HQ545/30, Chroma; eGFP/TagRFP-T: dichroic Di01-R488/561 and filter FF01-523/610, Semrock) was focused onto a back-illuminated electron multiplying CCD camera (iXon+, DU-897E-CSO-BV, Andor). Bright field illumination was achieved using the microscope source, coupled into the illumination objective using a dichroic (FF593-Di03, Semrock). The sample dish (Delta-T, Bioptech) is mounted onto a custom designed manual xy-stage, in which a thermal control unit (Delta-T, Bioptech) is integrated

to control the sample temperature (36°C). An objective heater (FAB6318x, 1000 Oaks Optical) aids in thermal control. A xyz-piezo stage (Nano-Bio3200, Mad City Labs), controlled by Labview software, is used for precision positioning and vertical scanning of the sample. Microscope, shutters and EMCCD camera are controlled by MetaMorph software.

Design of the cantilever holder

The cantilever holder consists of four stainless steel cylinders. The first unit is stably mounted to the objective, while the other units are successively connected via two miniature linear guides per plane (MR3MNSS1V0N15L-2.5-2.5, Precision Alliance), enabling movement of the fourth cylinder in three dimensions with respect to the objective. A micrometer drive (DM11-5, Newport) counteracted by a small spring is used for precise position control of each plane. The fourth cylinder holds a lug with a small groove that accommodates the AFM cantilever. High vacuum grease (Dow Corning) is used to reversibly fix the cantilever and ensures stable mounting after ~ 10 min settling time.

DNA constructs

The Halo-tag was purchased from Promega (pHTN HaloTag CMV-neo Vector), and SNAP-tag was purchased from New England Biolabs (pSNAPf-Vector). The mEos2-GR and mEos2-H4 constructs were generated by fusing GR to mEos2[41] in the pSNAPf vector (New England Biolabs). YPet[42], eGFP and Tag-RFP-T[43] fusion constructs were generated by using pLV-tetO-Oct4 as a backbone (kindly provided by Konrad Hochedlinger). Briefly, the Oct4 coding sequence was replaced with coding sequences of the different fusion proteins. All fusion constructs were generated as N-terminal fusions of the fluorescent protein to each protein of interest. The YPet-GR A458T mutant was generated by site-directed mutagenesis. To generate DNA-binding domain deletion mutants of GR, PCR products of sequences upstream and downstream of the DNA binding domain (as defined in the Uniprot database, http://www.uniprot.org/) were generated and ligated together. The primers used to make the different constructs can be found in Supplementary Table 2.

Generation of stable cell lines

MCF-7 cells stably expressing mEos2, mEos2-GR and mEos2-H4 were generated by transfection with Polyplus reagent and selected with puromycin for 2–3 weeks. All other cell lines were generated by lentiviral transduction. Briefly, each construct was cotransfected with the packaging plasmids MD2G and PAX2 (kindly provided by Didier Trono) in 293T cells using lipofectamine 2000. Supernatants were collected 48 hours after transfection and filtered through 0.45 μm low protein binding filters (Pall corporation). 1–2 ml of supernatant were used to transduce 3–5x10^4 U2-OS or MCF-7 cells, and the medium was changed 1–3 days after transduction.

Cell culture

U2-OS cells were cultured in high glucose DMEM (Gibco) supplemented with 10% fetal bovine serum (FBS), 1% penicillin/streptomycin and 2 mM GlutaMax (Gibco). MCF-7 were cultured in a-MEM (Gibco) supplemented with 10% FBS, 1% penicillin/streptomycin, 2

mM L-glutamine (Gibco), 1 mM sodium pyruvate and 100 mM non-essential amino acids (mMCF7). To achieve uninduced conditions for GR or ER, cells were grown at least one day in mMCF7 using charcoal stripped FBS (mMCF7-), and one day in mMCF7-without phenol-red. Just before imaging, OptiMEM was used to wash the cells once and maintain them for imaging. To induce the activity of GR and ER, cells were treated for 30 minutes with 100 nM dexamethasone or 100 nM β-estradiol, respectively. For the U2-OS cell lines stably expressing BMAL1 and CLOCK fusion constructs, cells were first synchronized by serum shock. Briefly, cells were first incubated in suspension in a 1:1 mix of complete culture medium and FBS for one hour before the medium was changed to complete cell culture medium (Phenol red-free DMEM supplemented with 10% fetal bovine serum (FBS), 1% penicillin/streptomycin and 2 mM L-glutamine (Gibco)). Cells were then further incubated for 24 hours before imaging and imaged without washing or change of buffer, except for the two-color experiments, where OptiMEM was used for imaging.

Determination of the laser beam profile

Before reflection, the laser beam profile was characterized by imaging the intensity cross-section at various distances from the focus onto the EMCCD camera, and determining the full width at half maximum (FWHM) from Gaussian fits to each intensity distribution. To characterize the beam profile after reflection, fluorescent beads (TetraSpeck microspheres, 100 nm diameter, Invitrogen) attached to fixed Hela cells for elevation above the sample surface were scanned across the beam at various distances from the focus, using the piezo xyz-stage. Fluorescence emitted by the beads was projected onto the EMCCD camera, and beads were kept in focus by moving the detection objective with a piezo z-stage (PIFOC, Physik Instrumente). The FWHM of the laser beam was determined from Gaussian fits to the resulting intensity distributions. Errors of the FWHM are the standard deviations of the parameter obtained from the fits.

Data acquisition

Cells were imaged in Delta-T glass bottom dishes (Bioptechs). Dishes were washed once with OptiMEM, and imaged in OptiMEM at 36°C for up to 45 min (GR and GR mutants), 60 min (uninduced ER) and 120 min (induced ER).

Data acquisition with RLSM is straightforward and comparable to other single molecule assays. Exchange of the AFM cantilever and positioning with respect to the light sheet focus can be achieved within 20 min. Once in place, a cantilever typically can be used for 5 days of imaging, with only minor position adjustments for each sample. Positioning of the cantilever next to a cell is precisely controlled by the xyz piezo stage and achieved within 1 min without perforating the cell membrane.

The power of all illumination lasers was kept below 3 mW, which corresponds to ~ 5 kW/cm^2 in the focal plane of the illumination objective. This is comparable to the laser power density used in other live cell single molecule microscopy assays[44].

Single molecule tracking

Single molecule tracking was achieved essentially as described[29]. In brief, images were background-subtracted using Matlab (2010b, Mathworks). After additional smoothing, the coarse position of fluorescent molecules was determined from pixel values exceeding a threshold of 4x standard deviation over the background. The fine position of particles was obtained by two-dimensional Gaussian fitting on the initial background-subtracted image.

Comparison of RLSM and HILO

Cells were imaged in OptiMEM at room temperature. The position, peak intensity and background level of single molecules was determined by two-dimensional Gaussian fitting on the original uncorrected image. The signal-to-background ratio (SBR) was defined as signal divided by the background level above the camera dark offset[45]. For both RLSM and HILO, the SBRs of all molecules within a nuclear z-section of a cell were combined into a histogram, whose median value was used to calculate the ratio between RLSM and HILO SBR for this z-section.

Extraction of diffusion components

In order to accurately determine the diffusion properties of labeled molecules from short tracks, arising from photobleaching or diffusion out of the focal plane, we analyzed cumulative distribution functions of squared displacements instead of the mean squared displacement[46]. The probability density $f(x^2+y^2)$ of squared displacements (x^2+y^2) for Brownian diffusion is given by

$$f\left(x^2+y^2\right)=\frac{1}{4\pi D\tau}\exp\left(-\frac{(x^2+y^2)}{4D\tau}\right),$$

where D denotes the diffusion constant and τ the camera integration time. Integration of the probability density yields the cumulative distribution function $F(x^2+y^2)$:

$$F(x^2+y^2)=\int\frac{1}{4\pi D\tau}\exp\left(-\frac{(x^2+y^2)}{4D\tau}\right)d(x^2+y^2)=\left(1-\exp\left(-\frac{(x^2+y^2)}{4D\tau}\right)\right), \quad (1)$$

or

$$F(X)=A_1\left(1-\exp\left(-\frac{X}{D_1}\right)\right)+A_2\left(1-\exp\left(-\frac{X}{D_2}\right)\right)+(1-A_1-A_2)\left(1-\exp\left(-\frac{X}{D_3}\right)\right) \quad (2)$$

in case of three different diffusion components, with $X = (x^2+y^2)/4\tau$.

To avoid bias towards slowly moving particles that remain visible for longer times, we only counted the first displacement of each track. To avoid false assignments of molecules to another track for fast molecules, we set an upper limit of 6 pixels for the maximum squared displacement of a molecule. This limit was accounted for by replacing the last term in Equation (2) with

$$(1-A_1-A_2)\left(\exp\left(-\frac{X}{D_3}\right)-\exp\left(-\frac{C_1}{D_3}\right)\right)/\left(\exp\left(-\frac{C_2}{D_3}\right)-\exp\left(-\frac{C_1}{D_3}\right)\right),$$

where the constants C_1 and C_2 are given by the lower and upper limits for the squared displacements of 0 and 6 pixels[47]. Fitting was performed in Igor Pro (v. 6.2, Wavemetrics), using a non-linear least squares fitting procedure. Errors are calculated as the standard deviation of parameters obtained from fits to 2000 random subsets of the displacements, each comprising 80% of the original data.

Determination of off-rate constants

We considered molecules localized for at least two consecutive frames within 0.5 pixels (1 pixel in two-color experiments) as bound molecules. Localizations only visible in one frame were discarded to avoid counting slowly moving molecules. We allowed one dark frame within a trajectory to account for rare blinking events of the fluorescent protein at an illumination time of 50 ms.

When monitoring a fluorescent bound transcription factor, the fluorescent signal (fluorescent 'on'-state) terminates due to two poisson-distributed processes, photobleaching with rate constant k_1 and dissociation with rate constant $k_2 = k_{off}$. The photobleaching rate k_1 is proportional to the light intensity, and thus dependent on the frame time τ_{int} and time-lapse time τ_{tl}, $k_1 = k_b \tau_{int}/\tau_{tl}$. Overall, the distribution of fluorescent 'on' times $f_1(t)$ follows an exponential function with the effektive off-rate constant $k_{eff} = (k_1 + k_2) = (k_b\ \tau_{int}/\tau_{tl} + k_{off})$:

$$f_1(t)=A\exp\left(-k_{eff}t\right)=A\exp\left(-\left(k_b\frac{\tau_{\mathrm{int}}}{\tau_{tl}}+k_{off}\right)t\right). \quad (3)$$

To obtain the dissociation rate constant k_{off}, Equation (3) was fitted to distributions of fluorescent 'on' times measured at different time-lapse times, yielding k_{eff}. $k_{eff}\ \tau_{\mathrm{tl}}$ was then plotted as function of the time-lapse time. In this graph, k_{off} is given by the slope and $k_b\ \tau_{\mathrm{int}}$ by the y-intersect.

Alternatively, we obtained the values for k_{off} and k_b by a global fit of Equation (3) to all fluorescent 'on' time distributions at different time-lapse times, yielding similar values.

If the linear extrapolation of k_{eff} deviates from a line, this suggests that two dissociation rate constants are resolved (Supplementary Fig. 5). In this case the distribution of fluorescent 'on' times was fit by the double-exponential function:

$$f_2(t)=A\left(B\exp\left(-\left(k_b\frac{\tau_{\mathrm{int}}}{\tau_{tl}}+k_{off,1}\right)t\right)+(1-B)\exp\left(-\left(k_b\frac{\tau_{\mathrm{int}}}{\tau_{tl}}+k_{off,2}\right)t\right)\right) \quad (4)$$

with dissociation rate constants $k_{off,1}$ and $k_{off,2}$. Here, B denotes the fraction of molecules unbinding with off-rate $k_{off,1}$. Errors for dissociation rate constants and amplitudes are the standard deviations of the parameters obtained from fits to Equation 3 or Equation 4.

Supplementary Material

Refer to Web version on PubMed Central for supplementary material.

Acknowledgments

We acknowledge W. Min for his contribution in the early stage of this work. The pLV-tetO-Oct4 plasmid was kindly provided by K. Hochedlinger (Department of Stem Cell and Regenerative Biology, Howard Hughes Medical Institute, Harvard Stem Cell Institute, Boston, MA, USA) and MD2G and PAX2 plasmids were kindly provided by D. Trono (Global Health Institute, School of Life Sciences, Ecole Polytechnique Federale de Lausanne (EPFL), Lausanne, Switzerland). Funding from NIH (X.S.X. (5RO1EB010244-3 and 5R01GM096450-02) and T.M. (R01NS043915 and DP1OD003930-03)), Human Frontier Science Program Organization (J.C.M.G.), fellowship for advanced researchers from the Swiss National Science Foundation (D.M.S.), Jane Coffin Childs postdoctoral fellowship (R.R.), National Science Scholarship from the Agency of Science, Technology and Research (A*STAR) of Singapore (Z.W.Z.) and Molecular Biophysics Training Grant Agency NIH/NIGMS T32 GM008313 (A.C.) is thankfully acknowledged. This work was performed in part at the Harvard Center for Nanoscale Systems (CNS), a member of the National Nanotechnology Infrastructure Network (NNIN), which is supported by the National Science Foundation under NSF award no. ECS-0335765.

References

1. Li GW, Xie XS. Central dogma at the single-molecule level in living cells. Nature. 2011; 475:308–315. [PubMed: 21776076]
2. McNally JG, Muller WG, Walker D, Wolford R, Hager GL. The glucocorticoid receptor: rapid exchange with regulatory sites in living cells. Science. 2000; 287:1262–1265. [PubMed: 10678832]
3. Fuda NJ, Ardehali MB, Lis JT. Defining mechanisms that regulate RNA polymerase II transcription in vivo. Nature. 2009; 461:186–192. [PubMed: 19741698]
4. Xie XS, Choi PJ, Li GW, Lee NK, Lia G. Single-molecule approach to molecular biology in living bacterial cells. Annu Rev Biophys. 2008; 37:417–444. [PubMed: 18573089]
5. Hammar P, et al. The lac repressor displays facilitated diffusion in living cells. Science. 2012; 336:1595–1598. [PubMed: 22723426]
6. Goulian M, Simon SM. Tracking single proteins within cells. Biophys Journal. 2000; 79:2188–2198.
7. Seisenberger G, et al. Real-time single-molecule imaging of the infection pathway of an adeno-associated virus. Science. 2001; 294:1929–1932. [PubMed: 11729319]
8. Sako Y, Minoghchi S, Yanagida T. Single-molecule imaging of EGFR signalling on the surface of living cells. Nat Cell Biol. 2000; 2:168–172. [PubMed: 10707088]
9. Tokunaga M, Imamoto N, Sakata-Sogawa K. Highly inclined thin illumination enables clear single-molecule imaging in cells. Nat Methods. 2008; 5:159–161. [PubMed: 18176568]
10. Huisken J, Swoger J, Del Bene F, Wittbrodt J, Stelzer EH. Optical sectioning deep inside live embryos by selective plane illumination microscopy. Science. 2004; 305:1007–1009. [PubMed: 15310904]
11. Friedrich M, et al. Detection of single quantum dots in model organisms with sheet illumination microscopy. Biochem and Biophys Res Comm. 2009; 390:722–727. [PubMed: 19833091]
12. Ritter JG, Veith R, Veenendaal A, Siebrasse JP, Kubitscheck U. Light sheet microscopy for single molecule tracking in living tissue. PLoS One. 2010; 5:e11639. [PubMed: 20668517]
13. Cella Zanacchi F, et al. Live-cell 3D super-resolution imaging in thick biological samples. Nat Methods. 2011; 8:1047–1049. [PubMed: 21983925]
14. Capoulade J, Wachsmuth M, Hufnagel L, Knop M. Quantitative fluorescence imaging of protein diffusion and interaction in living cells. Nat Biotechnology. 2011; 29:835–839.
15. Wu Y, et al. Inverted selective plane illumination microscopy (iSPIM) enables coupled cell identity lineaging and neurodevelopmental imaging in Caenorhabditis elegans. Proc of the Nat Acad of Sci. 2011; 108:17708–17713.
16. Planchon TA, et al. Rapid three-dimensional isotropic imaging of living cells using Bessel beam plane illumination. Nat Methods. 2011; 8:417–423. [PubMed: 21378978]

17. Tsai SY, et al. Molecular interactions of steroid hormone receptor with its enhancer element: evidence for receptor dimer formation. Cell. 1988; 55:361–369. [PubMed: 3167984]
18. Aagaard MM, Siersbaek R, Mandrup S. Molecular basis for gene-specific transactivation by nuclear receptors. Biochimica et biophysica acta. 2011; 1812:824–835. [PubMed: 21193032]
19. Huisken J, Stainier DY. Selective plane illumination microscopy techniques in developmental biology. Development. 2009; 136:1963–1975. [PubMed: 19465594]
20. Keppler A, et al. A general method for the covalent labeling of fusion proteins with small molecules in vivo. Nat Biotechnology. 2003; 21:86–89.
21. Los GV, et al. HaloTag: a novel protein labeling technology for cell imaging and protein analysis. ACS Chem Biol. 2008; 3:373–382. [PubMed: 18533659]
22. Mazza D, Abernathy A, Golob N, Morisaki T, McNally JG. A benchmark for chromatin binding measurements in live cells. Nucleic Acids Res. 2012
23. Manley S, et al. High-density mapping of single-molecule trajectories with photoactivated localization microscopy. Nat Methods. 2008; 5:155–157. [PubMed: 18193054]
24. English BP, et al. Single-molecule investigations of the stringent response machinery in living bacterial cells. Proc of the Nat Acad of Sci. 2011; 108:E365–373.
25. Speil J, et al. Activated STAT1 transcription factors conduct distinct saltatory movements in the cell nucleus. Biophys Journal. 2011; 101:2592–2600.
26. Akhtar A, Gasser SM. The nuclear envelope and transcriptional control. Nat Rev Genet. 2007; 8:507–517. [PubMed: 17549064]
27. Thompson RE, Larson DR, Webb WW. Precise nanometer localization analysis for individual fluorescent probes. Biophys Journal. 2002; 82:2775–2783.
28. Bancaud A, et al. Molecular crowding affects diffusion and binding of nuclear proteins in heterochromatin and reveals the fractal organization of chromatin. The EMBO Journal. 2009; 28:3785–3798. [PubMed: 19927119]
29. Elf J, Li GW, Xie XS. Probing transcription factor dynamics at the single-molecule level in a living cell. Science. 2007; 316:1191–1194. [PubMed: 17525339]
30. Becker M, et al. Dynamic behavior of transcription factors on a natural promoter in living cells. EMBO Rep. 2002; 3:1188–1194. [PubMed: 12446572]
31. Heck S, et al. I kappaB alpha-independent downregulation of NF-kappaB activity by glucocorticoid receptor. EMBO J. 1997; 16:4698–4707. [PubMed: 9303314]
32. Zava DT, Chamness GC, Horwitz KB, McGuire WL. Human breast cancer: biologically active estrogen receptor in the absence of estrogen? Science. 1977; 196:663–664. [PubMed: 193182]
33. Hong H, Kohli K, Trivedi A, Johnson DL, Stallcup MR. GRIP1, a novel mouse protein that serves as a transcriptional coactivator in yeast for the hormone binding domains of steroid receptors. Proc Natl Acad Sci U S A. 1996; 93:4948–4952. [PubMed: 8643509]
34. Beck M, et al. The quantitative proteome of a human cell line. Mol Syst Biol. 2011; 7:549. [PubMed: 22068332]
35. Gekakis N, et al. Role of the CLOCK protein in the mammalian circadian mechanism. Science. 1998; 280:1564–1569. [PubMed: 9616112]
36. Sprague BL, et al. Analysis of binding at a single spatially localized cluster of binding sites by fluorescence recovery after photobleaching. Biophys Journal. 2006; 91:1169–1191.
37. Beaudouin J, Mora-Bermudez F, Klee T, Daigle N, Ellenberg J. Dissecting the contribution of diffusion and interactions to the mobility of nuclear proteins. Biophys Journal. 2006; 90:1878–1894.
38. Mueller F, Mazza D, Stasevich TJ, McNally JG. FRAP and kinetic modeling in the analysis of nuclear protein dynamics: what do we really know? Curr Opin Cell Biol. 2010; 22:403–411. [PubMed: 20413286]
39. Stavreva DA, Varticovski L, Hager GL. Complex dynamics of transcription regulation. Biochimi et Biophys Acta. 2012
40. Mueller F, Morisaki T, Mazza D, McNally JG. Minimizing the impact of photoswitching of fluorescent proteins on FRAP analysis. Biophys Journal. 2012; 102:1656–1665.

41. McKinney SA, Murphy CS, Hazelwood KL, Davidson MW, Looger LL. A bright and photostable photoconvertible fluorescent protein. Nat Methods. 2009; 6:131–133. [PubMed: 19169260]
42. Nguyen AW, Daugherty PS. Evolutionary optimization of fluorescent proteins for intracellular FRET. Nat Biotechnol. 2005; 23:355–360. [PubMed: 15696158]
43. Shaner NC, et al. Improving the photostability of bright monomeric orange and red fluorescent proteins. Nat Methods. 2008; 5:545–551. [PubMed: 18454154]
44. Jones SA, Shim SH, He J, Zhuang X. Fast, three-dimensional super-resolution imaging of live cells. Nat Methods. 2011; 8:499–508. [PubMed: 21552254]
45. Moerner WE, Fromm DP. Methods of single-molecule fluorescence spectroscopy and microscopy. Rev Sci Instrum. 2003; 74
46. Schutz GJ, Schindler H, Schmidt T. Single-molecule microscopy on model membranes reveals anomalous diffusion. Biophys Journal. 1997; 73:1073–1080.
47. Gebhardt JCM, Clemen AE, Jaud J, Rief M. Myosin-V is a mechanical ratchet. Proc Natl Acad Sci USA. 2006; 103:8680–8685. [PubMed: 16731631]

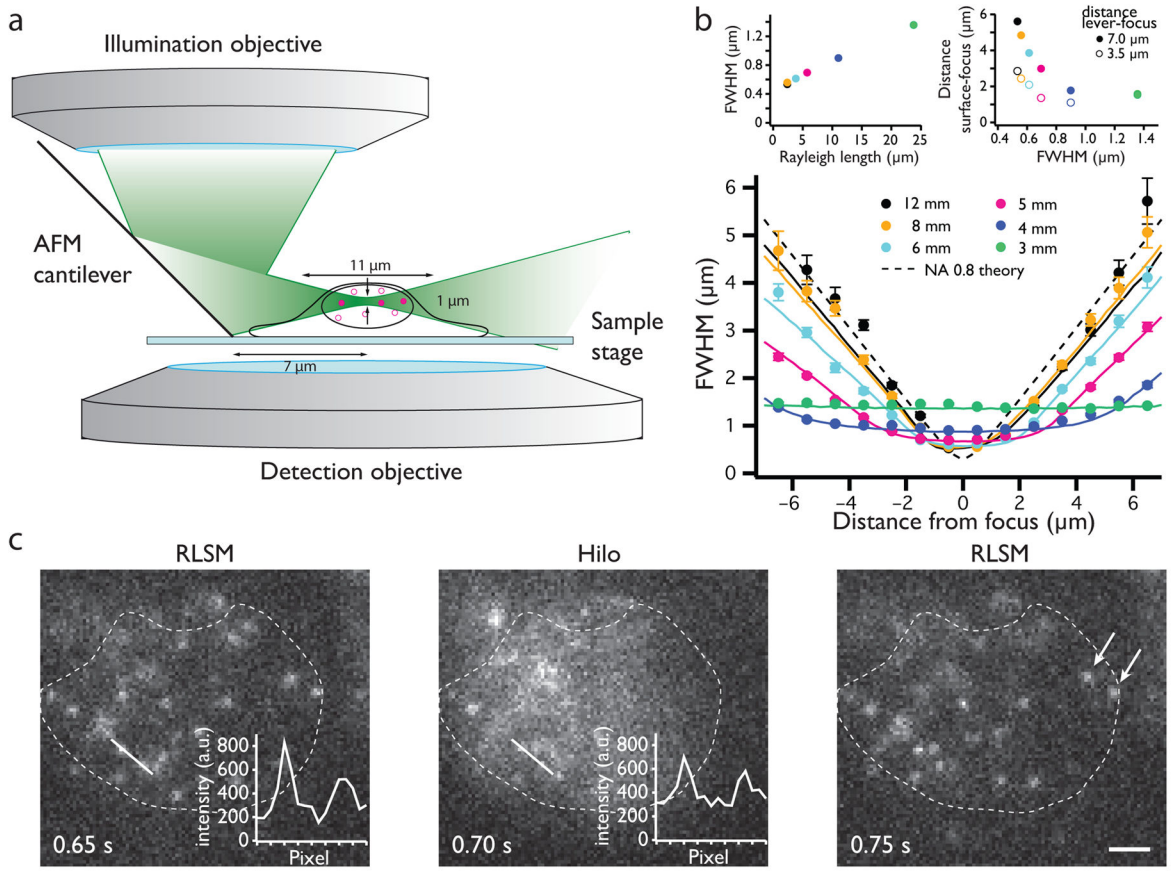

Figure 1.

Visualization of single fluorescently labeled DNA binding proteins by reflected light sheet microscopy. (**a**) Scheme of the reflected light sheet principle. A laser beam is focused by an objective to form a vertical light sheet that is reflected by 90° off an atomic force microscopy (AFM) cantilever next to a cell in a petri dish. Fluorescence is detected by a second high numerical aperture objective. 3D optical sectioning is achieved by vertical displacement of the sample. (not drawn to scale; see Supplementary Fig. 1) (**b**) Full width at half maximum (FWHM) of the light sheet before (solid lines) and after reflection (symbols) as function of the distance from the focus, shown at different aperture diameters. The dashed line indicates the beam profile expected for an objective with a numerical aperture of 0.8. Error bars represent ± s.d. (see online methods). Left inset: FWHM of the light sheet at the focus as a function of the Rayleigh length for different aperture diameters. Right inset: minimal distance between surface and focus as a function of the FWHM for different aperture diameters and distances between cantilever edge and focus. (**c**) Alternate RLSM and HILO images of a MCF-7 cell expressing mEos2-H4 with 50 ms time resolution ~ 6 µm above the coverslip. Insets in the left and middle panel indicate the fluorescence intensity along the white line. Arrows (right panel) indicate mEos2 molecules detected with RLSM but overlooked by HILO. The dashed line outlines the nuclear envelope. Scale bar is 2 µm.

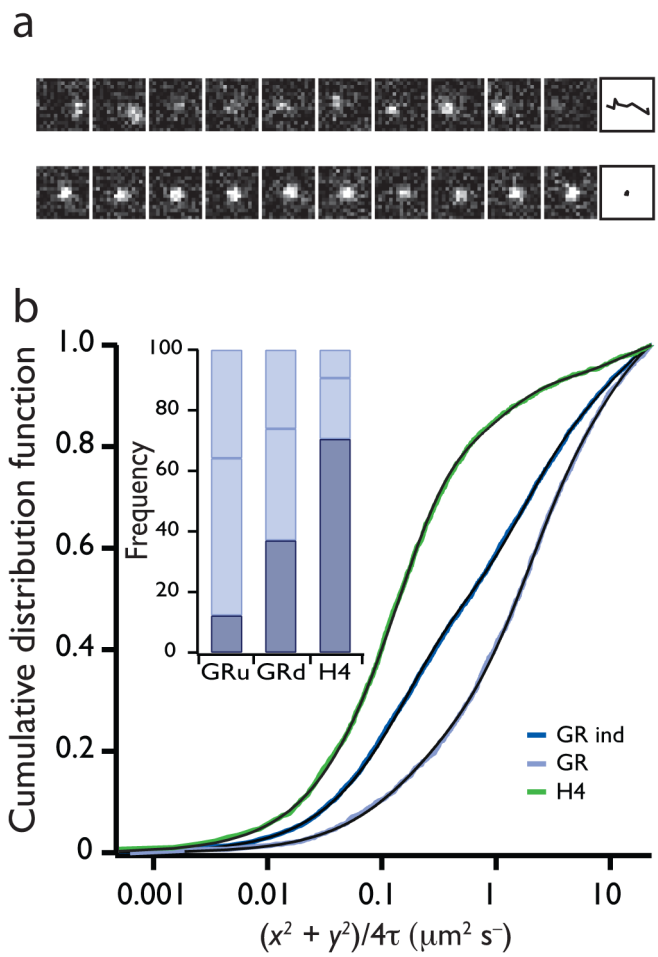

Figure 2.

Characterization of *in vivo* transcription factor diffusion. (**a**) Examples of single molecule tracking of a fast-diffusing mEos2-GR molecule (upper panel) and of a DNA-bound molecule (lower panel) in presence of 100 nM dexamethasone at 10 ms time resolution. (**b**) Cumulative distribution functions of squared displacements of mEos2-H4 and mEos2-GR without or with 100 nM dexamethasone treatment (n = 3336, 7 cells (GRd), n = 1644, 4 cells (GRu), n = 2020, 8 cells (H4)). Black lines indicate fits with three effective diffusion components to the distributions (Equation 2 in online methods). Inset: fractions of molecules exhibiting slow effective diffusion corresponding to DNA-bound fraction (dark blue) and molecules exhibiting fast effective diffusion (light blue).

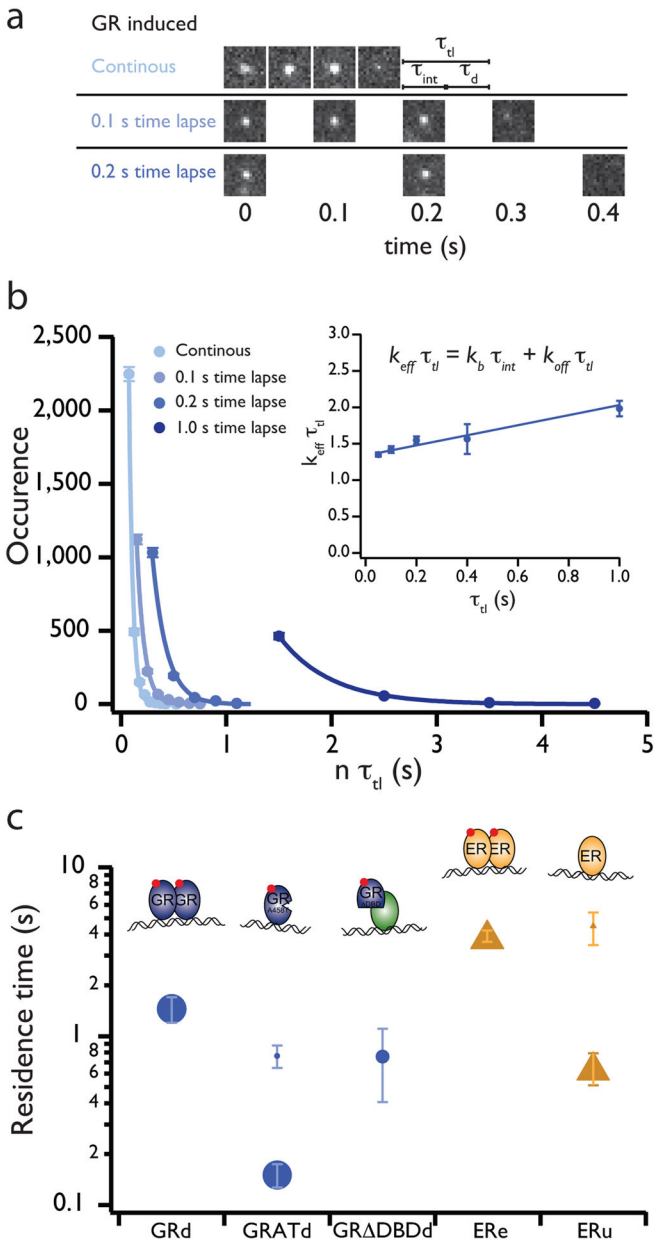

Figure 3.

Characterization of *in vivo* transcription factor residence times on DNA. (**a**) Images of single DNA-bound YPet-GR molecules during time-lapse imaging with various dark times. (**b**) Histograms of fluorescent 'on' times in different time-lapse conditions (n = 2991 (0.05 s), n = 1465 (0.1 s), n = 1308 (0.2 s), n = 92 (0.4 s), n = 539 (1.0 s), data from 34 cells). Lines are fits by an exponential decay model with one effective rate constant (Equation 3 in online methods). Inset: extracted effective rate constant as function of the time-lapse condition. Error bars represent ± s.d. k_{eff}: effective rate constant, k_b: photobleaching rate constant, k_{off}: off-rate constant, τ_{tl}: duration of time-lapse, τ_{int}: camera integration time, τ_d: dark time. (**c**) Residence times of dimeric GR (GRd), the point mutant GR A458T incapable of

dimerization (GRATd), and a mutant lacking the DNA binding domain (GRΔDBDd), all induced with 100 nM dexamethasone, and ER induced with 100 nM β-estradiol (ERe) or uninduced ER (ERu) in MCF-7 cells. Symbol size is proportional to the fraction of molecules exhibiting a certain residence time, or the number of binding events relative to GR for GR ΔDBD. The sketches illustrate the most abundant binding mode. Error bars represent ± s.d. (see online methods).

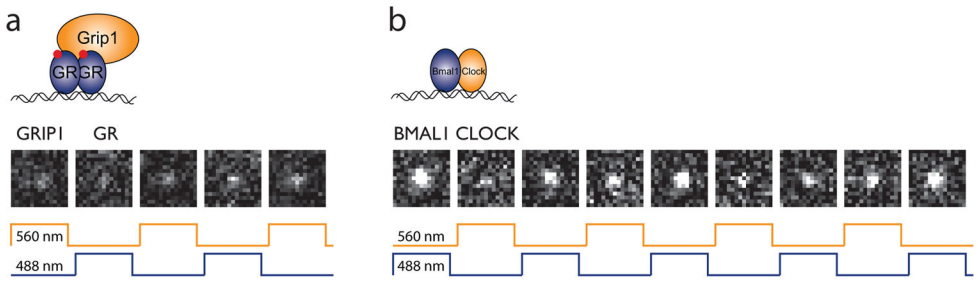

Figure 4.

Two-color imaging of two different molecular species at the single molecule level. (**a**) Example of GR/GRIP1 co-localization. TagRFP-T-GR (blue trace) and eGFP-GRIP1 (orange trace) were alternately excited with 50 ms exposure time. (**b**) Example of BMAL1/CLOCK co-localization. TagRFP-T-BMAL1 (blue trace) and eGFP-CLOCK (orange trace) were alternately excited with 50 ms exposure time.